Journal of Magnetic Resonance 214 (2012) 360–365

Contents lists available at SciVerse ScienceDirect

Journal of Magnetic Resonance

journal homepage: www.elsevier.com/locate/jmr

Communication

# Compressed sensing sodium MRI of cartilage at 7T: Preliminary study

Guillaume Madelin [a,c], Gregory Chang [a], Ricardo Otazo [b], Alexej Jerschow [c,*], Ravinder R. Regatte [a,*]

[a] Quantitative Multinuclear Musculoskeletal Imaging Group (QMMIG), Center for Biomedical Imaging, Radiology Department, New York University Langone Medical Center, New York, NY, USA
[b] Center for Biomedical Imaging, Radiology Department, New York University Langone Medical Center, New York, NY, USA
[c] Chemistry Department, New York University, New York, NY 10012, USA

ARTICLE INFO

*Article history:*
Received 24 August 2011
Revised 1 December 2011
Available online 13 December 2011

*Keywords:*
Sodium
Cartilage
Magnetic resonance imaging
Compressed sensing
Osteoarthritis

ABSTRACT

Sodium MRI has been shown to be highly specific for glycosaminoglycan (GAG) content in articular cartilage, the loss of which is an early sign of osteoarthritis (OA). Quantitative sodium MRI techniques are therefore under development in order to detect and assess early biochemical degradation of cartilage, but due to low sodium NMR sensitivity and its low concentration, sodium images need long acquisition times (15–25 min) even at high magnetic fields and are typically of low resolution. In this preliminary study, we show that compressed sensing can be applied to reduce the acquisition time by a factor of 2 at 7T without losing sodium quantification accuracy. Alternatively, the nonlinear reconstruction technique can be used to denoise fully-sampled images. We expect to even further reduce this acquisition time by using parallel imaging techniques combined with SNR-improved 3D sequences at 3T and 7T.
© 2011 Elsevier Inc. All rights reserved.

## 1. Introduction

Osteoarthritis (OA) is the most common form of arthritis in synovial joints and a leading cause of chronic disability, mainly in the elderly population. In 2008, it was estimated that nearly 27 million adults in the United States (9% of the population) have clinical OA. It is predicted that by the year 2030, nearly 67 million adults (19% of the US population) will be affected by OA [1,2]. There is no known cure for OA and present treatments focus mainly on pain management and ultimately, joint replacement. There are many obstacles to studying OA, including heterogeneity in etiology, variability in progression of disease, and long time periods required to see morphological and structural joint changes. Consequently, we currently lack the ability to predict the course of the disease in individual patients. Therefore, there is a high demand for the development of reliable, objective, non-invasive, and rapid quantitative imaging biomarkers. From a biochemical point of view, OA is a degenerative disease of articular cartilage and is mainly characterized by a loss of glycosaminoglycans (GAGs), a possible change in size and organization of collagen fibers, and by increased water content. Functional magnetic resonance imaging (MRI) techniques are under development to detect biochemical changes in cartilage such as $T_{1\rho}$ mapping [3], $T_2$ mapping [4], delayed Gadolinium-enhanced MRI of cartilage (dGEMRIC) [5], GAG chemical exchange saturation transfer (gagCEST) [6], diffusion MRI [7] and sodium ($^{23}$Na) MRI [8–10]. All these methods have their own advantages and disadvantages [11,12], but quantitative sodium MRI has been shown to be highly specific for the GAG content in cartilage [9,13,14]. Quantitative sodium MRI could therefore be used as a means of detection and assessment of the degree of biochemical degradation of cartilage in very early stages of OA [8–10,13–16]. Recent technological developments such as high magnetic field scanners, novel ultrashort echo time (UTE) pulse sequences, multi-channel radiofrequency (RF) arrays and non-Cartesian reconstruction methods have great potential for improving the performance of multinuclear imaging. However, due to the low sodium concentration in vivo and its low NMR sensitivity, imaging of sodium in cartilage still requires long acquisition times (15–20 min for usual sodium 3D images and 25 min for fluid suppressed images) with relatively low resolution [17–19].

Compressed sensing (CS) is a powerful method for image reconstruction which enables reduced imaging time by k-space undersampling. It has been under development since 2006 [20] and has been successfully applied to proton and $^{3}$He MRI [21–23], $^{13}$C and $^{19}$F spectroscopy [24,25], and to microfluidic flow imaging [26], as well as to combined time/k-space domain imaging [27–29]. CS is based on the sparsity (or compressibility) of the image in any known transform domain, the incoherence of the

* Corresponding authors. Address: Quantitative Multinuclear Musculoskeletal Imaging Group (QMMIG), Center for Biomedical Imaging, New York University Medical Center, 660 First Avenue, 4th Floor, New York, NY 10016, USA. Fax: +1 212 263 7541 (R.R. Regatte).

*E-mail addresses:* alexej.jerschow@nyu.edu (A. Jerschow), ravinder.regatte@nyumc.org (R.R. Regatte).

1090-7807/$ - see front matter © 2011 Elsevier Inc. All rights reserved.
doi:10.1016/j.jmr.2011.12.005

undersampling artifacts, and a dedicated nonlinear reconstruction algorithm. Sodium MRI of articular cartilage is intrinsically sparse and is therefore a good candidate for CS that should allow reconstruction of images from undersampled data within clinically feasible acquisition times (on the order of 10 min or less).

In this work, compressed sensing is applied to undersample a 3D radial pulse sequence for sodium MRI at high field (7T). The nonlinear reconstruction used in CS is also proposed to denoise fully-sampled images.

## 2. Materials and methods

### 2.1. Acquisition protocol

Data acquisition was performed in vivo on 4 asymptomatic volunteers (2 males, 2 females, average age: 36 ± 15 years) with a 3D radial sequence on a 7T whole-body scanner (Siemens Medical Solution, Erlangen, Germany), with a transmit/receive sodium RF knee coil (quadrature, birdcage) single-tuned at 78.6 MHz (Rapid MR International, Columbus), length 27 cm, and inner diameter 21 cm. Acquisition parameters for a fully sampled data set were: 10,000 projections, TE = 0.15 ms, TR = 100 ms, RF pulse flip angle = 90° of duration 500 μs, time of acquisition = 17 min. Note that the TE was calculated from the end of the RF pulse to the beginning of the data acquisition. The study was approved by the institutional review board and the volunteers signed an informed consent form prior to the experiment. The field-of-view (FOV) was chosen as 200 mm isotropic in order to keep a constant FOV for all volunteers who may have different knee sizes, and so that the calibration phantoms used for sodium quantification all lie within the FOV (see the Tissue Sodium Concentration (TSC) Quantification section).

### 2.2. Standard image reconstruction

Once the fully sampled data was acquired, images were reconstructed off-line in Matlab (Mathworks, Natick, MA, USA) with a non-uniform Fast Fourier Transform (NUFFT) regridding algorithm as described in [17,30,31]. All images were reconstructed as isotropic 100 × 100 × 100 voxels images, resulting in a nominal isotropic resolution of 2 mm. The R factors (acceleration rates) denote the degree of undersampling as follows:

- R = 1: Fully sampled data.
- R = 2, 3, 4: 50%, 33% and 25% of the radial projections were randomly chosen and kept from the original data; the other projections were assigned a value of 0. This random sampling was applied 100 times for each R factor (2, 3, and 4).

### 2.3. Compressed sensing (CS)

CS aims to accurately reconstruct certain signals and images from undersampled data acquired below the Nyquist rate. Three requirements are necessary to apply CS [20–22,32]:

(1) Sparsity: The desired image must have a sparse representation in a known transform domain (it must be compressible): it must be composed of a few high-value coefficients and many low-value coefficients, so that thresholding the low-value coefficients does not degrade the image quality too much. Usual sparsifying transforms are the discrete wavelet transform (DWT), discrete cosine transform (DCT), and finite differences. Sodium cartilage images acquired in this study are intrinsically sparse in the image domain as the strongest signals of interest occur only in ~20% of the voxels in the 3D image.

(2) Incoherence: The measurement basis and the sparse representation basis must be uncorrelated, so that the k-space undersampling artifacts add incoherently to the sparse signal coefficients. Thus, non-Cartesian data sampling is preferred for the design of sampling trajectories with low coherence. The 3D radial acquisition already fulfills this requirement as the spherical coordinates of the spokes in our acquisition scheme are chosen following the Rakhmanov–Saff–Zhou algorithm [33,34] in order to achieve a homogeneous distribution of the data along the radial views in a sphere. Most of the acquired data points are therefore away from the Cartesian grid.

(3) Nonlinear reconstruction: The image should be reconstructed by a nonlinear method that enforces both sparsity of the image representation in the transform domain and consistency of the reconstruction with the acquired samples. The image $\mathbf{x}$ is reconstructed from the acquired data $\mathbf{y}$ by minimizing the function $f(\mathbf{x})$:

$$f(x) = \|\mathcal{F}x - y\|_2^2 + \lambda_1 \|\Psi x\|_1 + \lambda_2 \mathrm{TV}(x), \tag{1}$$

where $\|x\|_1 = \sum_i |x_i|$ represents the $\ell_1$ norm, $\|x\|_2 = \sqrt{\sum_i |x_i|^2}$ is the $\ell_2$ norm, $\mathcal{F}$ denotes the (Cartesian) FFT, $\Psi$ is the sparsifying transform and TV($x$) represents the total variation of the image $\mathbf{x}$ (sum of the absolute variations of the image). Minimizing the $\ell_1$ norm promotes the sparsity while minimizing the $\ell_2$ norm enforces the data consistency. TV is a finite difference transform and it is often useful to add it as a penalty in order to increase the sparsity of the image in both the transform domain $\Psi$ and in the finite difference domain. $\lambda_1$ and $\lambda_2$ are weighting factors for the $\ell_1$ norm and TV respectively. Minimization of $f(\mathbf{x})$ was performed in Matlab (Mathworks, natick, MA, USA) using the nonlinear conjugate gradient method.

In this study, CS was applied on the normalized 3D regridded Cartesian k-space $\mathbf{y}$ of the images (after NUFFT reconstruction with R = 1, 2, 3 and 4), which was used for data consistency. The CS algorithm for reconstructing $\mathbf{x}$ was applied with 72 iterations and tested over a range of values for $\lambda_1$ and $\lambda_2$: $\lambda_1$ = 0.0005, 0.0010, 0.0025, 0.0050, 0.0075, 0.0100 and $\lambda_2$ = 0, 0.0005, 0.0010, 0.0025, 0.0050, 0.0075, 0.0100. The CS algorithm was tested with $\Psi = 1$ (no sparsifying transform) on all volunteers and also with $\Psi$ = DCT on one volunteer. The average reconstruction time for each pair $\lambda_1/\lambda_2$ was 5–10 min when $\Psi = 1$ and 9–20 min when $\Psi$ = DCT.

### 2.4. SNR measurements

Signal-to-noise ratio (SNR) measurement is a difficult task on images obtained from nonlinear reconstructions methods such as NUFFT and CS. In order to be able to fairly compare the SNR of images reconstructed with and without CS after NUFFT, 100 random samplings of the data were used to obtain more uniform distribution of the noise for all the images. The statistical standard deviation (STD) of all the voxels over these 100 randomly sampled reconstructed images was calculated for R = 2, 3 and 4, with and without CS applied after the NUFFT reconstruction. The distribution of the STD of noise (from 20 slices outside the knee anatomy) was very similar to a normal distribution (see Fig. 1, red fit) in all cases. This is to be expected for a large number of values ($N$ = 100) for which the STD is calculated (the $\chi^2$ distribution of STD becomes a normal distribution when $N > 50$ [35]). Note that since for $R = 1$ the full data cannot be randomly resampled, STD was extrapolated with a linear fit as a function of $\sqrt{\mathrm{R}}$ (see Fig. 2). The mean image (over 100 random samplings) was also calculated for $R$ = 2, 3, and 4. The mean signal in cartilage was then measured in selected ROIs of 30 voxels in 4 different regions in the cartilage

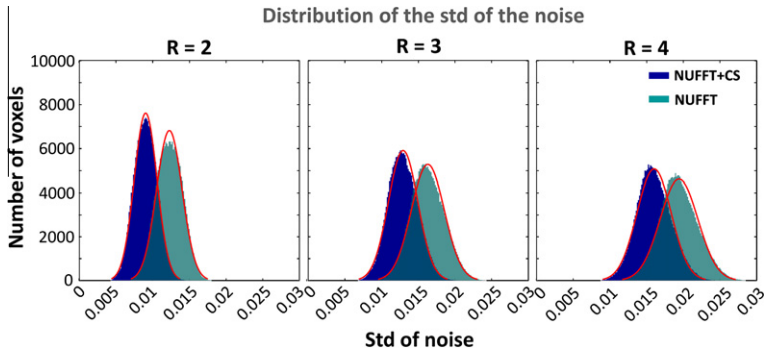


**Fig. 1.** Example of distribution of the standard deviations (STD) of the noise for $R = 2$, 3 and 4, for NUFFT (green) and NUFFT+CS (blue) and their best fit with a normal distribution (red curve), from one volunteer. Histograms were calculated from the STD of all the voxels of the 10 first and 10 last coronal slices of the 3D data (200,000 voxels) from one volunteer. STD of noise was calculated from 100 reconstructions with random sampling of the 10,000 acquired radial views for $R = 2$, 3 and 4. (For interpretation of the references to color in this figure legend, the reader is referred to the web version of this article.)

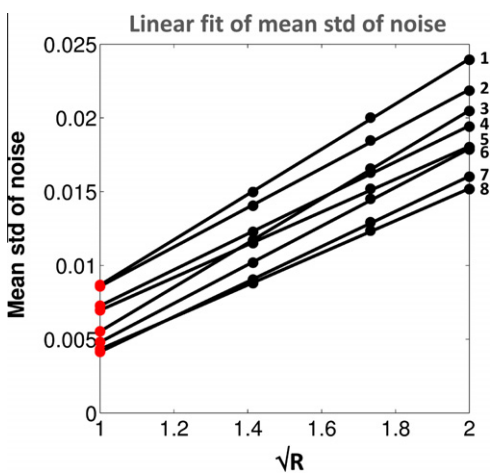


**Fig. 2.** Linear fit of mean STD of noise from data with $R = 2$, 3 and 4, for all 4 volunteers (Vol.), and 2 reconstruction methods (NUFFT and NUFFT+CS). Red dots: Extrapolated mean STD of the noise for $R = 1$ estimated from the linear fit of the data measured with $R = 2$, 3 and 4, as a function of $\sqrt{R}$. (1) Vol. 3, NUFFT. (2) Vol. 4, NUFFT. (3) Vol. 3, NUFFT+CS. (4) Vol. 2, NUFFT. (5) Vol. 1, NUFFT. (6) Vol. 4, NUFFT+CS. (7) Vol. 2, NUFFT+CS. (8) Vol. 1, NUFFT+CS. (For interpretation of the references to color in this figure legend, the reader is referred to the web version of this article.)

over 4 consecutive slices of these mean images. The cartilage regions were: patellar (abbreviation: PAT), femoro-tibial medial (MED), femoro-tibial lateral (LAT), and posterior femoral condyle (CON). The SNR of the images for each R was then calculated as: SNR = mean cartilage signal divided by mean STD of noise.

### 2.5. Tissue Sodium Concentration (TSC) quantification

The images were acquired with calibration tube phantoms that were placed on the knee cap and included in the FOV. Sodium quantitation was then performed using linear regression in Matlab as follows: ROIs were drawn in 4 calibration phantoms (150, 200, 250 and 300 mM NaCl) and their average signal intensities were corrected for T1, $T2^*_{short}$ and $T2^*_{long}$ of the gels as described in [17]. Another ROI was drawn in the noise area and the mean value of the noise was used as a 0 mM sodium concentration phantom. A linear regression curve of these corrected phantom intensities and noise versus sodium concentrations was then calculated and used to extrapolate the sodium 3D maps of the whole sample. After the regression curve calculation from the gel signals but before extrapolation of the images to sodium maps, the images were also corrected for the T1, $T2^*_{short}$ and $T2^*_{long}$ of cartilage measured in vivo [36]. As 75% of the volume in cartilage is extracellular and composed of water, and sodium ions are mainly present in this space, the sodium maps were divided by 0.75 in order to obtain the real sodium concentration [37,38]. Less than 5% of the cartilage volume is composed of cells [39] and the intracellular sodium concentration, estimated around 5-10 mM, can therefore be considered negligible in the present study.

Mean sodium concentrations in the 4 different regions of the cartilage were measured with exactly the same protocol used for measuring the signal (same slices, same ROIs) as described in the SNR measurements section.

### 2.6. Statistical analysis

For each volunteer and each region in cartilage, a Student's *t*-test was applied to the resulting sets of pixels (120 voxels) from the ROIs (30 voxels × 4 slices) on the TSC maps in order to compare all the CS data with the original fully sampled data (NUFFT, $R = 1$, without CS). Statistical significance was defined as the condition that $p < 0.05$.

## 3. Results and discussion

Examples of sodium images and TSC maps from one volunteer are shown in Figs. 3 and 4 on a coronal plane, for CS parameters $\lambda_1 = 0.0005$, $\lambda_2 = 0.0005$. Mean SNR and TSC measurements and p values over all volunteers are given in Tables 1 and 2. SNR was increased when CS was applied directly on fully sampled data for denoising (+69% on average), and slightly decreased for $R = 2$ data (−20% on average) compared to fully sampled data ($R = 1$). TSC of the cartilage looked very similar (within the standard deviation) within the 4 regions of cartilage for all R values, with and without CS applied, but these values are not a sufficient parameters to validate the accuracy of the measurements. CS data were considered as valid data for sodium quantification when both of the following conditions were fulfilled for all volunteers:

(1) All data were compared visually with the original fully sampled image (NUFFT, $R = 1$, without CS) in order to detect artifacts and local modifications of the signal that could be misinterpreted as a loss of sodium (such regions are indicated by arrows in Fig. 4 for $R = 3$ and 4). Most of the data with large TV weighting ($\lambda_2 > 0.0010$) were too blurred to give accurate estimation of the TSC and details in cartilage, and were therefore rejected.

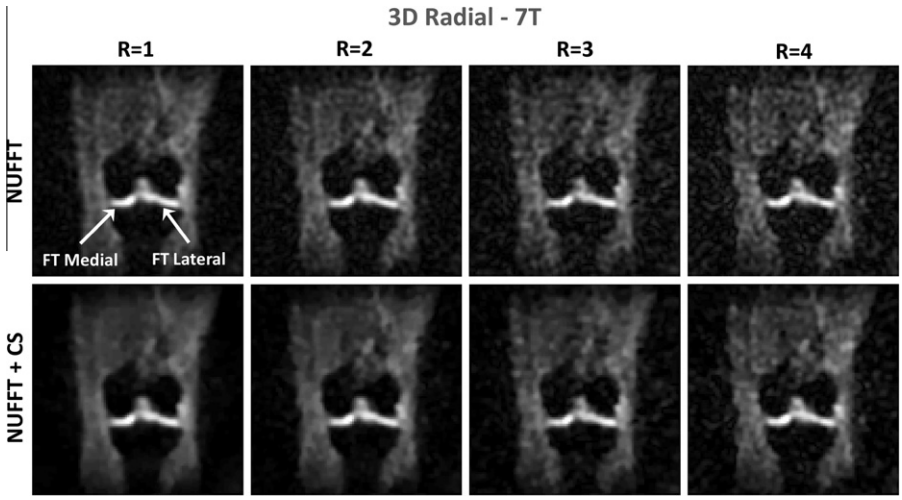


**Fig. 3.** Example of sodium images obtained from one volunteer with NUFFT without CS and with CS, with the parameters $\lambda_1 = 0.0005$, $\lambda_2 = 0.0005$ and $\Psi = 1$, for acceleration factors $R = 1$, 2, 3 and 4.

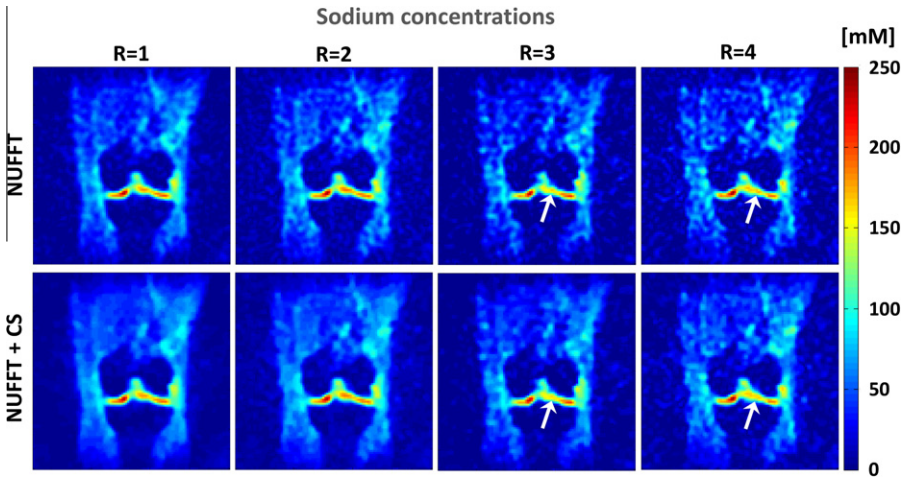


**Fig. 4.** Tissue Sodium Concentrations (TSC) in mM corresponding to the images shown in Fig. 3 obtained with NUFFT without CS and with CS, with the parameters $\lambda_1 = 0.0005$, $\lambda_2 = 0.0005$, for acceleration factors $R = 1$, 2, 3 and 4. The white arrows indicate zones in the femoro-tibial lateral cartilage where a loss of sodium concentration seems to appear in the data with $R = 3$ and 4 (with and without CS), and which could be misinterpreted as a loss of GAG in cartilage.

**Table 1**
Mean SNR in 4 regions of the cartilage for CS parameters: $\lambda_1 = 0.0005$, $\lambda_2 = 0.0005$ and $\Psi = 1$. Each mean ± standard deviation of SNR corresponds to the mean value over all volunteers of the SNR measured over four consecutive slices for each region and each volunteer. The values in the % columns correspond to the variation of SNR in % of the reference value for each column (NUFFT with $R = 1$). The numbers in bold correspond to the increased or equal SNR values compared to the reference SNR. Abbreviations: PAT = Patellar, MED = FT Medial, LAT = FT Lateral, CON = PF Condyle, with PF = Posterior Femoral, FT = Femoro-Tibial.

| SNR | | PAT | | MED | | LAT | | CON | |
|---|---|---|---|---|---|---|---|---|---|
| Recon. | $R$ | SNR | % | SNR | % | SNR | % | SNR | % |
| NUFFT | **1** | **43.8 ± 7.5** | **0** | **43.8 ± 6.2** | **0** | **42.5 ± 3.4** | **0** | **45.3 ± 6.4** | **0** |
| | **2** | 26.4 ± 4.5 | −40 | 26.3 ± 3.4 | −40 | 25.6 ± 2.1 | −40 | 27.3 ± 3.9 | −40 |
| | **3** | 19.9 ± 3.3 | −55 | 19.8 ± 2.6 | −55 | 19.2 ± 1.6 | −55 | 20.5 ± 2.9 | −55 |
| | **4** | 16.8 ± 2.9 | −62 | 16.9 ± 2.6 | −61 | 16.3 ± 1.3 | −62 | 17.5 ± 2.5 | −61 |
| NUFFT + CS | **1** | 73.9 ± 13.1 | **+69** | 74.4 ± 12.4 | **+70** | 71.7 ± 6.4 | **+69** | 76.7 ± 13.0 | **+69** |
| | **2** | 35.0 ± 6.2 | −20 | 35.2 ± 5.0 | −20 | 34.0 ± 2.9 | −20 | 36.3 ± 5.8 | −20 |
| | **3** | 24.5 ± 4.2 | −44 | 24.6 ± 3.5 | −44 | 23.8 ± 2.0 | −44 | 25.4 ± 3.9 | −44 |
| | **4** | 20.0 ± 3.5 | −54 | 20.2 ± 2.7 | −54 | 19.4 ± 1.6 | −54 | 20.9 ± 3.2 | −54 |

(2) Only CS data where the t-test showed a non-significant difference in all of the 4 regions of the cartilage compared to the fully sampled data were considered as valid. From this selection method, the only valid pairs of CS parameters $\lambda_1/\lambda_2$ were 0.0005/0, 0.0005/0.0005, 0.0010/0, for all volunteers (but also 0.0010/0.0005 and 0.0025/0 for 3 of them), for $\Psi = 1$, for $R = 1$, 2 and 4 only. When $\Psi$ = DCT, the only valid pairs of CS parameters $\lambda_1/\lambda_2$ were 0.0005/0 and 0.0005/0.0005, for $R = 1$, 2 and 4 only. CS data obtained from $R = 3$ always show a significant difference ($p < 0.05$) to fully sampled data in at least one part of the cartilage, for all the volunteers (see Table 2).

**Table 2**
Mean Tissue Sodium Concentration (TSC) in mM in four regions of the cartilage for CS parameters: $\lambda_1 = 0.0005$, $\lambda_2 = 0.0005$ and $\Psi = 1$. Each mean ± standard deviation of TSC corresponds to the mean value over all volunteers of the TSC measured over 4 consecutive slices for each region and each volunteer. The same regions of interests (ROIs) were used to compare measurements with different acceleration rates *R* for reconstruction. Mean *P* values over all volunteers were measured with a Student's *t*-test for comparing TSC measured in all voxels of the four ROIs (on four consecutive slices) to the reference data (NUFFT with R = 1). Abbreviations: PAT = Patellar, MED = FT Medial, LAT = FT Lateral, CON = PF Condyle, with PF = Posterior Femoral, FT = Femoro-Tibial.

| Recon. | *R* | PAT | *p* | MED | *p* | LAT | *p* | CON | *p* |
|---|---|---|---|---|---|---|---|---|---|
| NUFFT | **1** | **171 ± 42** | **1** | **172 ± 24** | **1** | **165 ± 3** | **1** | **160 ± 9** | **1** |
| | **2** | 171 ± 44 | 0.513 ± 0.161 | 174 ± 24 | 0.663 ± 0.204 | 165 ± 29 | 0.695 ± 0.301 | 161 ± 9 | 0.724 ± 0.255 |
| | **3** | 170 ± 40 | 0.037 ± 0.033 | 171 ± 22 | 0.545 ± 0.303 | 163 ± 27 | 0.472 ± 0.342 | 158 ± 7 | 0.571 ± 0.328 |
| | **4** | 171 ± 45 | 0.243 ± 0.192 | 173 ± 22 | 0.510 ± 0.265 | 165 ± 31 | 0.392 ± 0.369 | 162 ± 8 | 0.376 ± 0.297 |
| NUFFT + CS | **1** | 170 ± 42 | 0.600 ± 0.170 | 172 ± 24 | 0.882 ± 0.076 | 164 ± 27 | 0.624 ± 0.284 | 159 ± 9 | 0.833 ± 0.149 |
| | **2** | 171 ± 43 | 0.531 ± 0.236 | 173 ± 24 | 0.654 ± 0.179 | 164 ± 28 | 0.624 ± 0.247 | 160 ± 9 | 0.666 ± 0.171 |
| | **3** | 165 ± 39 | 0.014 ± 0.011 | 171 ± 23 | 0.592 ± 0.221 | 163 ± 27 | 0.335 ± 0.295 | 158 ± 7 | 0.549 ± 0.368 |
| | **4** | 170 ± 45 | 0.371 ± 0.374 | 173 ± 23 | 0.506 ± 0.212 | 164 ± 30 | 0.395 ± 0.249 | 161 ± 8 | 0.403 ± 0.228 |

Although $R = 4$ (with and without CS) can give some results similar to fully sampled data for the average TSC ($p > 0.05$), some parts of cartilage show a loss of sodium signal mainly due to reconstruction and undersampling that could be misinterpreted as a real loss of GAG, as shown on Fig. 4 (white arrows). $R = 3$ and 4 seem therefore to be too high undersampling rates and may lead to statistically significant differences in TSC measurements compared to fully sampled data and also to possible misinterpretation of the images. CS can therefore be used to either de-noise fully sampled data ($R = 1$) in order to increase the SNR and therefore potentially increase the accuracy in sodium quantification, or on undersampled data with $R = 2$ to decrease the total acquisition time without losing TSC accuracy. The application of a sparsifying transform such as DCT is not necessary for the present purpose, which is cartilage sodium imaging in the knee, as it generates similar results than $\Psi = 1$. The sodium cartilage images are sparse enough for applying CS on the image domain itself, and CS reconstruction is therefore faster (~5 min with $\Psi = 1$ instead of ~9 min with $\Psi$ = DCT).

For verification, the CS method was also applied on data acquired with undersampling rates $R = 1$ (8000 projections), $R = 2$ (4000 projections) and $R = 4$ (2000 projections) on another volunteer, and the resulting images were compared to the images obtained from the CS method applied to simulated R factors on fully sampled data as described in the Materials and Methods\Standard Image Reconstruction section. Both methods showed identical results.

## 4. Conclusion

This preliminary study shows that CS can be applied to sodium MRI of cartilage at 7T in order to decrease the acquisition time by a factor of two without losing accuracy in TSC over different regions of interest in the cartilage for detecting early signs of OA. Further studies will involve testing the application of the CS technique to data acquired at 3T, with and without fluid suppression at both 3T and 7T, combined with new 3D radial based sequences such as density adapted 3D radial [40], Twisted projection imaging (TPI) [41] or 3D cones [42] which allow increases in SNR. Further improvements could be obtained by combining CS with NUFFT in the iterative process (as $\mathcal{F}$ in Eq. (1)), instead of simply working with the Cartesian k-space (obtained after one NUFFT reconstruction) for the data consistency part of Eq. (1). This step, however, is by no means obvious, as the NUFFT algorithm applied from Cartesian to radial data can induce errors that can propagate during the CS algorithm, and as a result reduce the efficiency of the technique.

A further improvement, upon acquisition of multichannel double-tuned ($^1$H + $^{23}$Na) RF knee coils at 3T and 7T, would be to apply CS Sodium MRI in combination with parallel imaging to further reduce the imaging time by another factor 2 or 3. Such approaches are already under development in our center for dynamic proton MRI [43,44].

## Acknowledgment

This research work was supported by NIH Grants R01 AR053133, R01 AR056260 and R01 AR060238.

## References

[1] R. Lawrence, D. Felson, C. Helmick, L. Arnold, H. Choi, R. Deyo, S. Gabriel, R. Hirsch, M. Hochberg, G. Hunder, et al., Estimates of the prevalence of arthritis and other rheumatic conditions in the United States: Part II, Arthritis Rheum. 58 (1) (2008) 26–35.
[2] H. Kotlarz, C. Gunnarsson, H. Fang, J. Rizzo, Insurer and out-of-pocket costs of osteoarthritis in the US: evidence from national survey data, Arthritis Rheum. 60 (12) (2009) 3546–3553.
[3] R. Regatte, S. Akella, A. Borthakur, J. Kneeland, R. Reddy, In vivo proton MR three-dimensional T1$\rho$ mapping of human articular cartilage: initial experience, Radiology 229 (1) (2003) 269.
[4] T. Mosher, B. Dardzinski, Cartilage MRI T2 relaxation time mapping: overview and applications, in: Seminars in Musculoskeletal Radiology, vol. 8, 2004, pp. 355–368.
[5] A. Bashir, M. Gray, D. Burstein, Gd-DTPA2-as a measure of cartilage degradation, Magn. Reson. Med. 36 (5) (1996) 665–673.
[6] W. Ling, R. Regatte, G. Navon, A. Jerschow, Assessment of glycosaminoglycan concentration in vivo by chemical exchange-dependent saturation transfer (gagCEST), Proc. Natl. Acad. Sci. 105 (7) (2008) 2266.
[7] L. Filidoro, O. Dietrich, J. Weber, E. Rauch, T. Oerther, M. Wick, M. Reiser, C. Glaser, High-resolution diffusion tensor imaging of human patellar cartilage: feasibility and preliminary findings, Magn. Reson. Med. 53 (5) (2005) 993–998.
[8] R. Reddy, E. Insko, E. Noyszewski, R. Dandora, J. Kneeland, J. Leigh, Sodium MRI of human articular cartilage in vivo, Magn. Reson. Med. 39 (5) (1998) 697–701.
[9] E. Shapiro, A. Borthakur, A. Gougoutas, R. Reddy, 23Na MRI accurately measures fixed charge density in articular cartilage, Magn. Reson. Med. 47 (2) (2002) 284–291.
[10] L. Wang, Y. Wu, G. Chang, N. Oesingmann, M. Schweitzer, A. Jerschow, R. Regatte, Rapid isotropic 3D-sodium MRI of the knee joint in vivo at 7T, J. Magn. Reson. Imaging 30 (3) (2009) 606–614.
[11] R. Regatte, M. Schweitzer, Novel contrast mechanisms at 3 Tesla and 7 Tesla, Semin. Musculoskelet. Radiol. 12 (3) (2008) 266–280.
[12] G. Gold, C. Chen, S. Koo, B. Hargreaves, N. Bangerter, Recent advances in MRI of articular cartilage, Am. J. Roentgenol. 193 (3) (2009) 628.
[13] L. Lesperance, M. Gray, D. Burstein, Determination of fixed charge density in cartilage using nuclear magnetic resonance, J. Orthop. Res. 10 (1) (1992) 1–13.
[14] A. Borthakur, E. Mellon, S. Niyogi, W. Witschey, J. Kneeland, R. Reddy, Sodium and T1$\rho$ MRI for molecular and diagnostic imaging of articular cartilage, NMR Biomed. 19 (7) (2006) 781–821.
[15] A. Borthakur, E. Shapiro, J. Beers, S. Kudchodkar, J. Kneeland, R. Reddy, Sensitivity of MRI to proteoglycan depletion in cartilage: comparison of sodium and proton MRI, Osteoarthr. Cartilage 8 (4) (2000) 288–293.
[16] E. Shapiro, A. Borthakur, R. Dandora, A. Kriss, J. Leigh, R. Reddy, Sodium visibility and quantitation in intact bovine articular cartilage using high field 23Na MRI and MRS, J. Magn. Reson. 142 (1) (2000) 24–31.

[17] G. Madelin, J. Lee, S. Inati, A. Jerschow, R. Regatte, Sodium inversion recovery MRI of the knee joint in vivo at 7T, J. Magn. Reson. 207 (2010) 42–52.
[18] G. Madelin, A. Jerschow, R. Regatte, Sodium MRI with fluid suppression: will it improve early detection of osteoarthritis?, Imaging Med 3 (1) (2011) 1–4.
[19] R. Higgs, Osteoarthritis: concentrated efforts to detect early OA, Nat. Rev. Rheumatol. 6 (11) (2010) 616.
[20] E. Candès, J. Romberg, T. Tao, Robust uncertainty principles: exact signal reconstruction from highly incomplete frequency information, Inf. Theory IEEE Trans. 52 (2) (2006) 489–509.
[21] M. Lustig, D. Donoho, J. Pauly, Sparse MRI: the application of compressed sensing for rapid MR imaging, Magn. Reson. Med. 58 (6) (2007) 1182–1195.
[22] M. Lustig, D. Donoho, J. Santos, J. Pauly, Compressed sensing MRI, Signal Process. Mag. IEEE 25 (2) (2008) 72–82.
[23] S. Ajraoui, K. Lee, M. Deppe, S. Parnell, J. Parra-Robles, J. Wild, Compressed sensing in hyperpolarized 3He Lung MRI, Magn. Reson. Med. 63 (4) (2010) 1059–1069.
[24] S. Hu, M. Lustig, A. Balakrishnan, P. Larson, R. Bok, J. Kurhanewicz, S. Nelson, A. Goga, J. Pauly, D. Vigneron, 3D compressed sensing for highly accelerated hyperpolarized 13C MRSI with in vivo applications to transgenic mouse models of cancer, Magn. Reson. Med. 63 (2) (2010) 312–321.
[25] T. Kampf, A. Fischer, T. Basse-Lüsebrink, G. Ladewig, F. Breuer, G. Stoll, P. Jakob, W. Bauer, Application of compressed sensing to in vivo 3D 19F CSI, J. Magn. Reson. 207 (2010) 262–273.
[26] J. Paulsen, V. Bajaj, A. Pines, Compressed sensing of remotely detected MRI velocimetry in microfluidics, J. Magn. Reson. 205 (2) (2010) 196–201.
[27] M. Lustig, J. Santos, D. Donoho, J. Pauly, kt sparse: high frame rate dynamic mri exploiting spatio-temporal sparsity, in: Proceedings of the 13th Annual Meeting of ISMRM, Seattle, 2006, p. 2420.
[28] U. Gamper, P. Boesiger, S. Kozerke, Compressed sensing in dynamic MRI, Magn. Reson. Med. 59 (2) (2008) 365–373.
[29] H. Jung, K. Sung, K. Nayak, E. Kim, J. Ye, k–t focuss: a general compressed sensing framework for high resolution dynamic MRI, Magn. Reson. Med. 61 (1) (2009) 103–116.
[30] L. Greengard, J. Lee, Accelerating the nonuniform fast Fourier transform, SIAM Rev. 46 (3) (2004) 443–454.
[31] L. Greengard, J. Lee, S. Inati, The fast SINC transform and image reconstruction from nonuniform samples in k-space, Commun. Appl. Math. Comput. Sci. 1 (1) (2006) 121–131.
[32] E. Candès, M. Wakin, An introduction to compressive sampling, Signal Process. Mag. IEEE 25 (2) (2008) 21–30.
[33] E. Saff, A. Kuijlaars, Distributing many points on a sphere, Math. Intell. 19 (1) (1997) 5–11.
[34] E. Rakhmanov, E. Saff, Y. Zhou, Minimal discrete energy on the sphere, Math. Res. Lett. 1 (6) (1994) 647–662.
[35] G. Box, J. Hunter, W. Hunter, Statistics for experimenters: design, innovation, and discovery, second ed., 2005.
[36] G. Madelin, A. Jerschow, R. Regatte, Sodium relaxation times in the knee joint in vivo at 7T, NMR in Biomedicine XX (XX) (2011) XX–XX, in print.
[37] E. Shapiro, A. Borthakur, J. Kaufman, J. Leigh, R. Reddy, Water distribution patterns inside bovine articular cartilage as visualized by 1H magnetic resonance imaging, Osteoarthr. Cartilage 9 (6) (2001) 533–538.
[38] A. Borthakur, E. Shapiro, S. Akella, A. Gougoutas, J. Kneeland, R. Reddy, Quantifying sodium in the human wrist in vivo by using MR imaging1, Radiology 224 (2) (2002) 598.
[39] K. Kuettner, Biochemistry of articular cartilage in health and disease, Clin. Biochem. 25 (3) (1992) 155–163.
[40] A. Nagel, F. Laun, M. Weber, C. Matthies, W. Semmler, L. Schad, Sodium MRI using a density-adapted 3D radial acquisition technique, Magn. Reson. Med. 62 (6) (2009) 1565–1573.
[41] F. Boada, J. Gillen, G. Shen, S. Chang, K. Thulborn, Fast three dimensional sodium imaging, Magn. Reson. Med. 37 (5) (1997) 706–715.
[42] P. Gurney, B. Hargreaves, D. Nishimura, Design and analysis of a practical 3D cones trajectory, Magn. Reson. Med. 55 (3) (2006) 575–582.
[43] R. Otazo, D. Sodickson, Distributed compressed sensing for accelerated MRI, in: Proc. Intl. Soc. Mag. Reson. Med., vol. 17, 2009, p. 377.
[44] R. Otazo, D. Kim, L. Axel, D. Sodickson, Combination of compressed sensing and parallel imaging for highly accelerated first-pass cardiac perfusion MRI, Magn. Reson. Med. 64 (3) (2010) 767–776.